Monthly Notices
of the
ROYAL ASTRONOMICAL SOCIETY

Mon. Not. R. Astron. Soc. **425,** 1245–1256 (2012) doi:10.1111/j.1365-2966.2012.21510.x

Orbital and physical parameters of eclipsing binaries from the All-Sky Automated Survey catalogue – IV. A 0.61 + 0.45 $M_\odot$ binary in a multiple system

K. G. Hełminiak,[1,2]★ M. Konacki,[2,3] M. Różyczka,[4] J. Kałużny,[4] M. Ratajczak,[2] J. Borkowski,[2] P. Sybilski,[2] M. W. Muterspaugh,[5,6] D. E. Reichart,[7] K. M. Ivarsen,[7] J. B. Haislip,[7] J. A. Crain,[7] A. C. Foster,[7] M. C. Nysewander[7] and A. P. LaCluyze[7]

[1]*Departamento de Astronomía y Astrofísica, Facultad de Física, Pontificia Universidad Católica de Chile, Av. Vicuña Mackenna 4860, 782-0436 Macul, Santiago, Chile*
[2]*Nicolaus Copernicus Astronomical Center, Department of Astrophysics, ul. Rabiańska 8 , 87-100 Toruń, Poland*
[3]*Astronomical Observatory, A. Mickiewicz University, ul. Słoneczna 36, 60-286 Poznań, Poland*
[4]*Nicolaus Copernicus Astronomical Center, ul. Bartycka 18, 00-716 Warszawa, Poland*
[5]*Department of Mathematics and Physics, College of Engeneering, Tennessee State University, Boswell Science Hall, Nashville, TN 37209, USA*
[6]*Tennessee State University, Center of Excellence in Information Systems, 3500 John A. Merritt Blvd., Box No. 9501, Nashville, TN 37203-3401, USA*
[7]*Department of Physics and Astronomy, University of North Carolina, Campus Boc 3255, Chapel Hill, NC 27599-3255, USA*

Accepted 2012 June 12. Received 2012 June 8; in original form 2011 December 21

ABSTRACT

We present the orbital and physical parameters of a newly discovered low-mass detached eclipsing binary from the All-Sky Automated Survey (ASAS) data base: ASAS J011328–3821.1 A, which is a member of a visual binary system with the secondary component separated by about 1.4 arcsec. The radial velocities have been calculated from the high-resolution spectra obtained with the 1.9-m Radcliffe telescope/Grating Instrument for Radiation Analysis with a Fibre-Fed Echelle (GIRAFFE) spectrograph, the 3.9-m Anglo-Australian Telescope (AAT)/University College London Echelle Spectrograph (UCLES) and the 3.0-m Shane telescope/Hamilton Spectrograph (HamSpec) on the basis of the TODCOR technique and the positions of the H_α emission lines. For the analysis, we have used *V*- and *I*-band photometry obtained with the 1.0-m Elizabeth telescope and the 0.41-m Panchromatic Robotic Optical Monitoring and Polarimetry Telescopes (PROMPT), supplemented with the publicly available ASAS light curve of the system.

We have found that ASAS J011328–3821.1 A is composed of two late-type dwarfs, which have masses of $M_1 = 0.612 \pm 0.030$ $M_\odot$ and $M_2 = 0.445 \pm 0.019$ $M_\odot$ and radii of $R_1 = 0.596 \pm 0.020$ $R_\odot$ and $R_2 = 0.445 \pm 0.024$ $R_\odot$. Both show a substantial level of activity, which manifests in strong H_α and H_β emission and the presence of cool spots. The influence of the third light on the eclipsing pair properties has also been evaluated and the photometric properties of component B have been derived. A comparison with several popular stellar evolution models shows that the system is on its main-sequence evolution stage and that it is probably more metal-rich than the Sun. We have also found several clues to suggest that component B itself is a binary composed of two nearly identical ∼0.5-$M_\odot$ stars.

Key words: binaries: eclipsing – binaries: spectroscopic – binaries: visual – stars: fundamental parameters – stars: individual: ASAS J010538–3821.1 – stars: low-mass.

1 INTRODUCTION

In the last decade, there has been a stunning increase in our knowledge of the structure and evolution of eclipsing binaries. The number of known and well-studied detached low-mass eclipsing systems, which are the main sources of absolute parameter measurements,

★E-mail: xysiek@astro.puc.cl

has increased by almost an order of magnitude since the year 2000. This increase has helped several authors to make conclusions about a 30-yr-old problem: the discrepancy between observed and theoretically predicted radii and temperatures during the evolution of low-mass stars (Lacy 1977). The prevailing idea is that this discrepancy is caused by the stellar magnetic field, amplified by the fast rotation resulting from tidal locking in close binaries, which inhibits the efficiency of convection in the envelope and manifests itself in a higher level of activity than for single stars (Chabrier, Gallardo & Baraffe 2007). However, the number of known well-characterized systems is too low to reliably test this hypothesis. This is especially true among long-period systems, which normally exhibit lower levels of activity, so the observed radii and temperatures are closer to the theoretically predicted values. In a very recent paper, Irwin et al. (2011) have described an eclipsing pair of M dwarfs on a 41-d orbit. Despite having slow asynchronous rotation and a probable age over 120 Myr, these still show cold spots, and their radii are inflated by 5 per cent with respect to theoretical predictions. This system is evidence against the theory mentioned above, and it might again encourage wider interest in the need to revisit the equation of state for low-mass stars, which was suggested to explain the inflated radii before the activity hypothesis (e.g. Torres & Ribas 2002).

To be useful for testing the evolutionary models, the parameters of the system, especially masses and radii, should be known with a precision of at least 3 per cent, which is now considered to be a canonical level (Blake et al. 2008; Clausen et al. 2008). There are two other criteria that can make a system more interesting: (i) additional multiplicity – by deriving properties of the third body, it is possible to put additional constraints on the nature of the whole system; (ii) low-mass ratio – in general, it is harder to fit a single isochrone to data points that are well separated in parameter space (these are usually stars of different masses). Twin stars commonly have data points that lie close together and are less difficult to fit. In this paper, we present our analysis, together with the orbital and physical parameters of a newly discovered low-mass detached eclipsing binary that meets the two above-mentioned criteria. The data we gathered fell short of the 3 per cent precision-level goal, but the system is still highly valuable for our understanding of the nature of low-mass stars.

2 THE ASAS J011328–3821.1 SYSTEM

The eclipsing system ASAS J011328–3821.1 (2MASS J01132817–3821024, 1RXS J011328.8–382059, hereafter ASAS-01) has the shortest orbital period of all the objects in our sample of low-mass detached eclipsing binaries (LMDEBs; see: Hełminiak & Konacki 2011; Hełminiak et al. 2011) found in the All-Sky Automated Survey (ASAS) Catalogue of Variable Stars (ACVS; Pojmański 2002),[1] and it is one of the shortest among the LMDEBs known to date (i.e. $P_{\rm ASAS} = 0.44559$ d). In the ACVS, ASAS-01 is classified as eclipsing detached (ED) with a maximum brightness of $V = 11.78$ mag and an amplitude of brightness variation of 0.33 mag. The ASAS light curve clearly shows that there is a significant difference in the eclipse depths, which implies that the eclipsing pair is composed of two vastly different stars.

Before the ACVS, the object was not reported to be a binary or multiple, but it was noted as an X-ray source in the *Einstein* (Gioia et al. 1990; Stocke et al. 1991) and *ROSAT* (Voges et al. 1999) catalogues. Later, Beers et al. (1996) noted emission in calcium H and K lines, which they described in their catalogue as 'moderate to strong'. More recently, Riaz, Gizis & Harvin (2006) have identified ASAS-01 as an M0.5 dwarf, and they have given values of spectral indices CaH1, CaH2, CaH3 and TiO5. They have reported the H_α emission line with an equivalent width (EW) of 2.5 Å, and they have estimated the distance to be about 37 pc. This determination is significantly different from the value of 26.6 pc obtained by Szczygieł et al. (2008), who derived it on the basis of a bolometric correction derived from the ASAS $V - I$ colour. However, the object was treated as a single star, which explains the discrepancy.

The emission in H_α was recently confirmed by Parihar et al. (2009), who estimated the spectral types of components to be M1V + M3V. However, their study did not reflect the possibility of the system being composed of three or more stars.

Finally, in their lucky-imaging survey of southern M dwarfs, Bergfors et al. (2010) have obtained high-angular-resolution images of the system in the i' and z' bands. They have clearly separated two components, with the secondary located 1.405(3) arcsec at the position angle of 29.0(3) degrees. They have estimated the spectral types to be M0 + M1, not taking into account the eclipsing nature of one of the stars.

We have deduced the multiple nature of ASAS-01 in two ways. First, we noted that in the spectrum taken with the Shane telescope in 2007 (Section 3), the H_α emission-line profile was found to be triple. The same feature was found in a spectrum obtained in 2008 with the Anglo-Australian Telescope (AAT), but not in data obtained in 2006 with the Radcliffe telescope in South Africa. Shortly thereafter, and independent of Bergfors et al. (2010), we found the two components clearly separated on the CCD images obtained with the Elizabeth telescope in South Africa (Section 4) in good seeing conditions. Part of our image is shown in Fig. 1. The fainter component B is located about 1.25 arcsec from the brighter A in the north-east

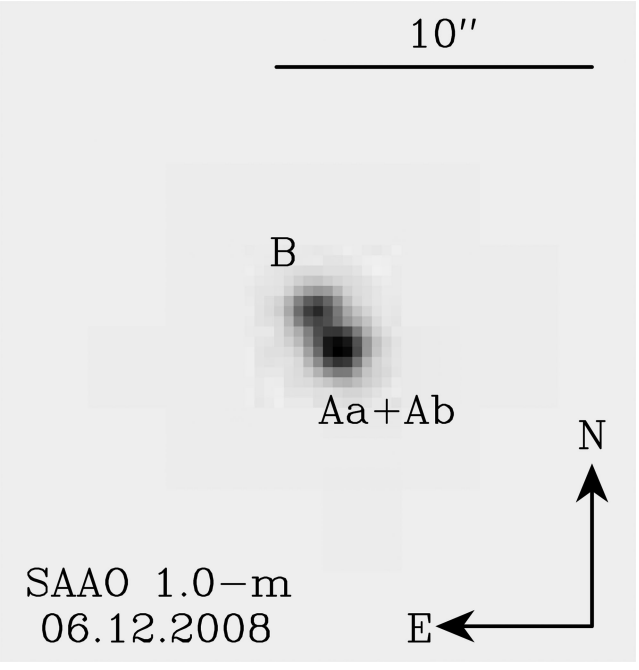

Figure 1. Part of an image taken with the 1.0-m Elizabeth telescope at SAAO, showing the two components of the ASAS-01 AB system. The visible components are separated by ∼1.25 arcsec. ASAS-01 Aa + Ab is a low-mass eclipsing detached binary identified in the ASAS data base ($P_{\rm ASAS} = 0.44559$ d). The orientation and the scale of the image are shown.

[1] http://www.astrouw.edu.pl/asas/?page=acvs

direction, which is consistent with the more precise result obtained by Bergfors et al. (2010). A series of images taken in different orbital phases (with respect to the photometric 0.44559-d period) has allowed us to deduce that eclipses occur in component A.

3 SPECTROSCOPY AND RADIAL VELOCITIES

3.1 Observations

To directly derive the masses of the components of ASAS-01, we obtained a series of high-resolution spectra in order to measure their radial velocities (RVs). Most of the spectroscopic observations come from the 1.9-m Radcliffe telescope and its Grating Instrument for Radiation Analysis with a Fibre-Fed Echelle (GIRAFFE) spectrograph at the South African Astronomical Observatory (SAAO), with settings the same as described in the previous papers of this series (Hełminiak et al. 2009, 2011). Five spectra of $R \sim 40\,000$ were obtained during three consecutive nights in 2006 September. After 3600 s of exposure and binning to $R \sim 10\,000$, we obtained the signal-to-noise (S/N) ratio at $\lambda = 6520$ Å between 25 and 40. At that time, we were not aware that the system is also a visual binary, and the quality of the image from the acquisition camera was not enough to demonstrate this. Because of relatively high seeing (about 2 arcsec and more), our spectra were contaminated by component B.

One additional spectrum was obtained in 2007 October with the 3.0-m Shane telescope and its Hamilton Spectrograph (HamSpec) at the Lick Observatory. The target was observed very low over the horizon for 2100 s. After binning from the original resolution of 60 000 to 30 000, we reached the S/N ratio level around 25 at $\lambda =$ 6560 Å. Because of the low S/N ratio, fringing, telluric lines and the limited extent of available templates, we did not use all 96 rows of the spectrum, but we used only 21 that covered the wavelength range from 5150 to 6500 Å. This spectrum was also contaminated by the light from component B.

The last spectrum was obtained in 2008 September with the 3.9-m AAT and its University College London Echelle Spectrograph (UCLES) at the Siding Spring Observatory, with the same settings as described in Hełminiak et al. (2009, 2011). This spectrum was not binned, and after 900 s of exposure we reached S/N ratio ∼20 at $\lambda = 6530$ Å. We tried to keep the slit on component A only, by rotating it by 90° from the position angle of the AB pair. However, because of the high seeing (over 2 arcsec), we could not avoid a significant contamination from star B.

3.2 Derivation of radial velocities

The CCD reduction, spectrum extraction and wavelength calibration were done in every case with standard IRAF procedures.[2] For the wavelength calibration, we used exposures of ThAr lamps taken before and after the science exposure. Initially, the RVs were measured with our implementation of the two-dimensional cross-correlation technique (TODCOR; Zucker & Mazeh 1994) using the spectrum of an M2V standard star HIP 93101, broadened to $v_{\rm rot}\sin i = 30$ km s^{-1}, which was taken as a template. The formal RV measurement errors were computed from the bootstrap analysis of the TODCOR maps created by adding randomly selected single-order TODCOR maps.

In the TODCOR maps, the location of the maximum of the cross-correlation function in the v_1/v_2 plane refers to the RVs of the two components of the system. We could easily phase-fold our measurements of the primary v_1 with the photometric period of 0.44559 d, but we failed when trying to do this for v_2 (putative secondary). Thus, to obtain the RV curve of the eclipsing secondary, we decided to measure the positions of the H_α emission lines. In all GIRAFFE spectra, we could easily recognize two well-separated components of that line and measure their positions, despite the fact that the line was close to the edge of an echelle order. To measure the positions, we used the `deblend` procedure in the IRAF/ECHELLE package and we fitted a double-Gaussian function. The fit was performed about 20 times with different initial wavelength range selections, initial peak positions and smoothing factors. The results were then averaged and the standard deviation was taken as the measurement error. A similar procedure was applied to the HamSpec and UCLES spectra but with a triple-Gaussian function, because the triple character of the H_α line was obvious. We did not normalize the spectra to the continuum before this procedure.

To check whether the RVs obtained from H_α lines can be trusted, we tried to phase-fold them separately with the photometric period. For the primary, we found a good agreement with the TODCOR measurements, and for the secondary we succeeded in finding a fit with the desired period, a systemic velocity close to that found for the primary and an amplitude K_2 significantly higher than that of the primary K_1. This is expected for two distinctive late-type dwarfs, considering the difference in the depths of the eclipses in the ASAS light curve. For the final orbital fit, we used all measurements simultaneously. We used the spectroscopic orbit fitting procedure described in our previous papers (Hełminiak et al. 2009; Hełminiak & Konacki 2011; Hełminiak et al. 2011). This simple code uses a Levenberg–Marquardt minimalization algorithm to find a Keplerian orbit of a spectroscopic binary. It also allows for estimation of systematic contributions to the error budget by Monte Carlo and bootstrap analysis.

3.3 ASAS-01 A orbital fit

Before obtaining the orbital fit, we used our photometric measurements (Section 4) to correct the ASAS ephemeris. Using the JKTEBOP and PHOEBE codes (see Section 5), we found a new value of the orbital period $P = 0.44559604(18)$ d and we incorporated it into the orbital fit. We have also found (from the photometry and RVs) that the eccentricity e agrees with zero well within formal errors, so we held it fixed later. We found the same for the difference between the systemic velocities of the primary and secondary $\gamma_{\rm Aa} - \gamma_{\rm Ab}$, and for any possible systematic shifts between v_1 measurements from TODCOR and H_α lines. However, the reduced χ^2 of the best-fitting solutions made separately for the H_α measurements of either the primary or the secondary were not close to 1. This means that the measurement errors were underestimated, so we added in quadrature a systematic term of 6.5 km s^{-1} to the formally derived measurement errors. This operation was not necessary for the TODCOR results. We also excluded one H_α measurement of the primary from the GIRAFFE spectrum at JD∼245 4008.477 and both from the UCLES spectrum, because of their very large formal uncertainties. The measurements from the UCLES spectrum probably also suffered from the line blending. For this exposure, the velocity difference was the smallest in the whole sample and the emission from

[2] IRAF is written and supported by the IRAF programming group at the National Optical Astronomy Observatories (NOAO) in Tucson, AZ (http://iraf.noao.edu/). NOAO is operated by the Association of Universities for Research in Astronomy (AURA), Inc. under cooperative agreement with the National Science Foundation.

Table 1. Single RV measurements of all components of the ASAS-01 system, derived with the TODCOR technique and from the position of the H_α emission lines, together with their formal errors and final orbital fit residua. R/G, S/H and A/U denote data points from Radcliffe/GIRAFFE observations, from the Shane/HamSpec spectrum and from AAT/UCLES, respectively. For component B, the residua refer to the fit of a circular orbit with $P_B \simeq 0.475$ d. When O − C is not given, the measurement is not included in the fit.

JD-245 0000	v (km s^{-1})	± (km s^{-1})	O − C (km s^{-1})	T/S
Component Aa velocities from TODCOR				
4006.50332	−86.882	4.360	3.502	R/G
4007.52761	98.787	7.240	3.361	R/G
4007.57128	140.808	7.037	7.444	R/G
4008.47697	140.128	4.695	3.230	R/G
4008.52042	112.337	4.540	−6.065	R/G
4375.87729	−100.752	8.175	−1.146	S/H
4727.14578	68.250	1.247	0.076	A/U
Component Aa velocities from H_α lines				
4006.50332	−90.330	6.971	0.054	R/G
4007.52761	96.905	7.435	1.479	R/G
4007.57128	132.301	6.895	−1.063	R/G
4008.47697	122.606	7.232	–	R/G
4008.52042	107.616	6.577	−10.786	R/G
4375.87729	−110.900	6.563	−11.295	S/H
4727.14578	94.415	6.540	–	A/U
Component Ab velocities from H_α lines				
4006.50332	161.590	7.509	−7.093	R/G
4007.52761	−85.570	7.401	1.556	R/G
4007.57128	−144.540	7.134	−5.276	R/G
4008.47271	−136.700	7.866	6.691	R/G
4008.52042	−113.824	7.176	4.881	R/G
4375.87729	191.210	6.655	9.812	S/H
4727.14578	−68.139	6.525	–	A/U
Component B velocities from TODCOR				
4006.50332	116.254	6.240	3.502	R/G
4007.52761	28.122	1.500	3.361	R/G
4007.57128	−21.130	6.076	7.444	R/G
4008.47697	19.200	3.690	3.230	R/G
4008.52042	−24.688	9.086	−6.065	R/G
4375.87729	−12.785	5.925	−1.147	S/H
4727.14578	21.381	0.482	0.076	A/U
Component B velocities from H_α lines				
4375.87729	13.147	6.587	–	S/H
4727.14578	6.799	6.633	–	A/U

component B is strongest. However, we believe that the TODCOR measurement is secure because the peak was very high and well separated from other smaller maxima.

All the RV measurements for all components of the ASAS-01 multiple system are listed in Table 1. For ASAS-01 A, we show only the measurements that were taken to produce the orbital fit and the final model of the system, together with their final errors and residuals. For component B, we show all the TODCOR v_2 values and two H_α velocities derived from HamSpec and UCLES spectra. In the T/S column, R/G denotes Radcliffe/GIRAFFE, S/H denotes Shane/HamSpec and A/U denotes AAT/UCLES telecope/spectrograph.

In the left panel of Fig. 2, we present all the measurements together with the best-fitting orbital solution obtained for the ASAS-01 A eclipsing pair. We have found the solution with a fast procedure that fits a double-Keplerian orbit by minimizing the χ^2 function using a Levenberg–Marquard method. The rms of the fit is 5.8 km s^{-1} for the primary and 7.0 km s^{-1} for the secondary. The final reduced χ^2 is 0.988, and thus we believe that the parameter uncertainties are well estimated. To ensure the accuracy of the estimates, we have also performed an additional Monte Carlo simulation to estimate the systematic errors of the derived parameters. The resulting systematic terms are an order of magnitude smaller than the formal ones, but they have been added in quadrature to the errors from the least-squares fit.

The orbital parameters derived from the fit are listed in Table 2. We can see that the H_α and TODCOR measurements are complementary and, when combined, they allow us to reach about a 2 per cent level of precision in the velocity amplitudes $K_{1,2}$ and about 4 per cent in $M \sin^3 i$. We would like to emphasize the low value of the mass ratio $q = 0.727(18)$, which makes ASAS-01 A unique. With this q, ASAS-01 A resides in the mass-ratio distribution of spectroscopic binaries well outside both the narrow peak at $q \gtrsim 0.95$ (the 'strong' twin hypothesis; Lucy 2006) and the wide peak at $q \gtrsim 0.85$ (the 'weak' twin hypothesis; Halbwachs et al. 2003). This makes ASAS-01 A particularly interesting for testing the evolutionary models.

3.4 Component B

The positions of the third H_α emission peak in the HamSpec and UCLES spectra are close to (but not in good agreement with) the corresponding measurements of v_2 from TODCOR. This has led to the conclusion that the v_2 coordinate of the TODCOR maxima might be related to component B, not the secondary component of the eclipsing Aa+Ab pair. If so, component B itself must be a spectroscopic binary, because the v_2 values change significantly by about 150 km s^{-1}. However, the third emission H_α peak is not clearly visible in the GIRAFFE spectra, so we cannot fully support this hypothesis by comparing all TODCOR and H_α measurements. Nevertheless, it is worth noticing that during two consecutive nights, when two R/G observations were taken with roughly 1 h time-span (JD∼245 4007.5 and 245 4008.5), the position of the peak on the TODCOR map changed by about 45 km s^{-1}. The remaining R/G spectrum (JD∼245 4006.5) – from which the highest value of v_2 was derived (116 km s^{-1}) – had the highest signal-to-noise ratio.

From the TODCOR measurements of component B's RVs, we have derived an acceptable orbital solution with the rms of measurements of 7.1 km s^{-1} and a reduced χ^2 of the fit of nearly 3. The parameters of this solution are listed in Table 3, and the model RV curve along with the single measurements and residua (listed in Table 1) are plotted in the right panel of Fig. 2. In this orbital fit, we have not included the measurements derived from the H_α lines, because the resulting parameters are not very different from the ones given, and the quality of the fit (in terms of rms and χ^2) is substantially worse. We can see that the systemic velocity γ_B differs from the value of γ_A by less than the sum of their errorbars, which is expected in the case of gravitational bounding. This is an argument for the correctness of this fit and thus the binary nature of ASAS-01 B, but considering the amount and quality of the available data, we are far from making any conclusive statements about this hypothesis. The binarity of ASAS-01 B is discussed in a later part of the paper.

3.5 H_α line profiles

The existence of strong H_α emission is a manifestation of a substantial stellar activity in all components of the ASAS-01 system.

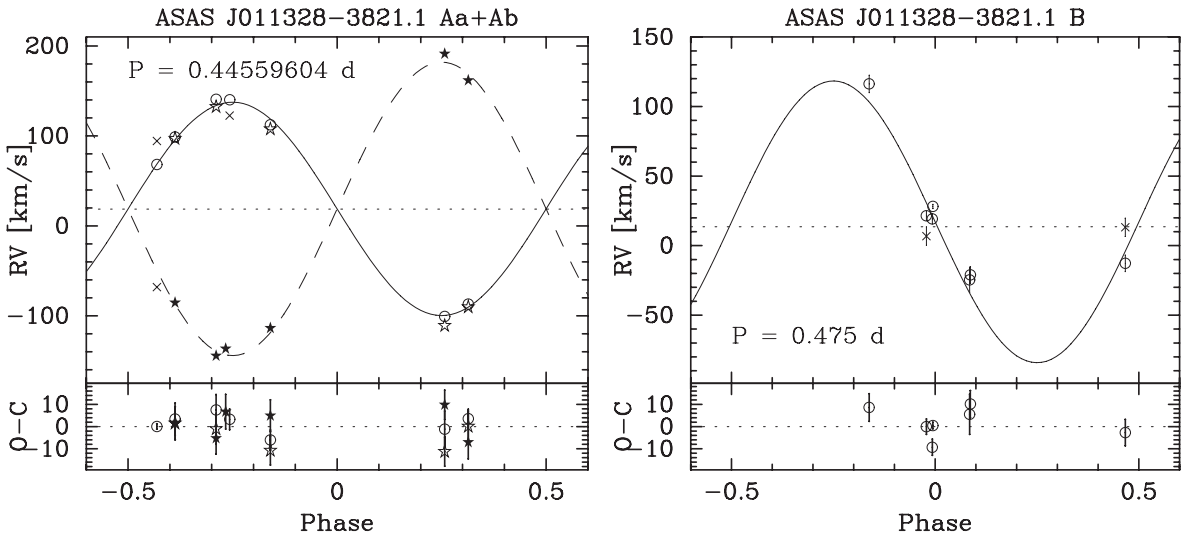

Figure 2. Left: RV measurements and the best-fitting orbital solution for the ASAS-01 A eclipsing binary. The open symbols and solid line are for the primary, and the filled symbols and dashed line are for the secondary. Circles denote TODCOR, stars denote H_α line measurements and crosses denote measurements rejected from the final fit. The residua with the final error bars are shown in the lower panel. Right: RV measurements of the ASAS-01 B component from the TODCOR technique and the best fit of a putative circular orbit with a period $P \simeq 0.475$ d. Crosses mark measurements rejected from the final fit. Residua and error bars are shown in the lower panel.

Table 2. Orbital parameters of the ASAS-01 A eclipsing binary. Note that the values of P and T_0 are taken from the simultaneous spectroscopic and photometric analysis performed with PHOEBE.

Parameter	Value	±
P_A (d)	0.44559604	1.8e-7
$T_{0,A}$ (JD-245 0000)	1868.83933	3.1e-4
K_{Aa} (km s^{-1})	118.4	2.0
K_{Ab} (km s^{-1})	162.9	3.3
γ_A (km s^{-1})	18.6	2.3
q_A	0.727	0.018
$a_A \sin i$ ($R_\odot$)	2.478	0.034
e_A	0.0	(fix)
$M_{Aa} \sin^3 i$ ($M_\odot$)	0.595	0.027
$M_{Ab} \sin^3 i$ ($M_\odot$)	0.432	0.017

Table 3. Parameters of the ASAS-01 B putative orbit.

Parameter	Value	±
P_B (d)	0.4750	0.0009
$T_{0,B}$ (JD-245 0000)	4806.950[a]	0.022
K_{Ba} (km s^{-1})	104.7	5.7
γ_B (km s^{-1})	13.6	2.9
e_B	0.0	(fix)
$a_{Ba} \sin i$ ($R_\odot$)	0.983	0.053
$f(M_{Ba})$ ($M_\odot$)	0.0565	0.0092

[a] T_0 is calculated for the moment of the orbital conjunction.

A closer inspection of the H_α lines reveals their probable variability. Fig. 3 presents the H_α profiles from all of our spectra. On the spectra from HamSpec and UCLES, all three components are clearly visible and marked. We must remember that, for the GIRAFFE setting, the H_α line was close to the edge of the echelle order, so the S/N ratio around the line was lower. For every spectrum, we measured the H_α EW; these are given in Table 4.

The Aa component seems to be particularly strong in both GIRAFFE spectra from September 30 (JD∼245 4008.5). This could be a result of either the real increase of the line intensity or the blending with component B. However, in the latter case, the velocity of component B calculated from the line position would differ by 50–70 km s^{-1} from the maximum on the corresponding TODCOR map. In the case of GIRAFFE data, the intensity and even the existence of the third peak are highly dependent on how the spectrum was normalized to the continuum. The low S/N ratio of the GIRAFFE spectra and the high rotational broadening of the stellar lines make this operation quite challenging and its results unreliable, especially at the orders' edges (i.e. around the H_α line).

The EW measurements, given in Table 4, were made under assumption of three emission components for all spectra, but we stress that for the R/G observation this assumption might be wrong because of the low S/N ratio. However, this data set shows a systematic decrease of the EW measurements for component B (by a factor of ∼2), and a rising trend for component Aa (by a factor of nearly 3). The EW_{Ab} values seem to be randomly oscillating around a constant value. Nevertheless, these measurements are not secure and they should be treated with caution.

In the HamSpec and UCLES observations, component B is obviously stronger than in the observations performed with GIRAFFE. The Aa component shows values substantially different between the two spectra. The EW_{Ab} for the HamSpec spectrum is within the oscillations seen in the GIRAFFE data, but in the UCLES spectrum it reaches the smallest value of all data sets. However, this might be because of the blending with component B. Given the activity of the system, we expect the observed variability of H_α to be real, but the quality of the data does not allow for a firm statement.

We also want to note that in three of the five GIRAFFE spectra, as well as in the HamSpec and UCLES observations, we have found signatures of H_β emission lines. Especially in the UCLES spectrum, the emission from all three components is clear and the EW measurements were possible. The shape of the profile is very similar to the H_α line. We found EWs to be 0.70, 0.17 and 0.62 Å for the Aa, Ab and B components, respectively, with an uncertainty

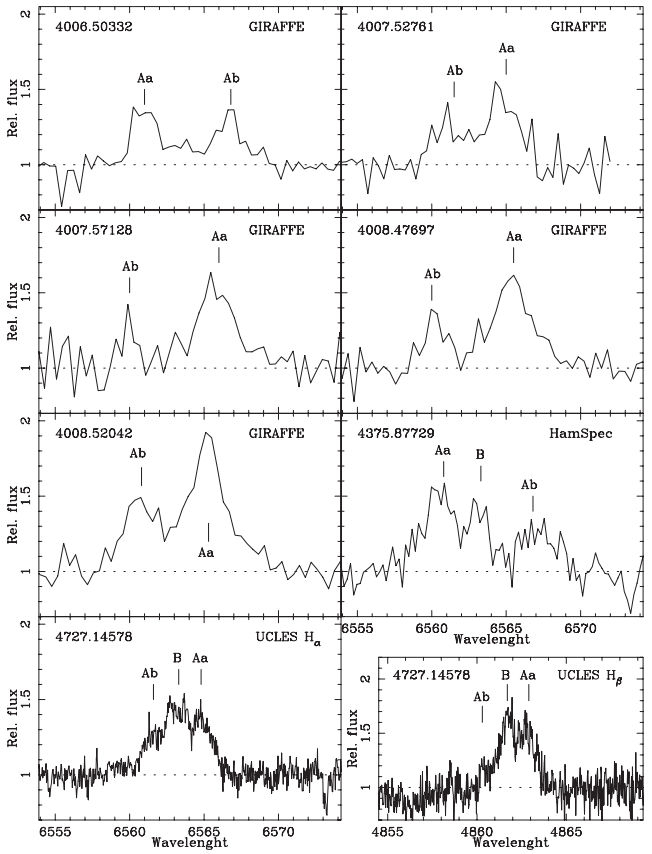

Figure 3. The H_α emission profile variability as seen in our spectra, especially for component B. For the GIRAFFE set-up, the H_α line is close to the order's edge, so the S/N ratio around it is very poor, which makes the continuum correction and EW calculations challenging. The H_β line from the UCLES spectrum is also shown for comparison. JD-245 0000 and spectrographs are labelled, and components are marked. The spectra are continuum normalized.

Table 4. H_α line EW measurements for all our spectra. The measurement errors are estimated to be around 0.1 Å. The values for component B from the GIRAFFE spectra (R/G) should be treated with caution.

JD 245 0000	EW_{Aa} (Å)	EW_{Ab} (Å)	EW_B (Å)	T/S
4006.50332	0.74	0.54	0.18	R/G
4007.52761	1.38	0.71	0.15	R/G
4007.57128	1.39	0.40	0.13	R/G
4008.47697	1.69	0.65	0.10	R/G
4008.52042	2.04	0.58	<0.1	R/G
4375.87729	1.60	0.67	0.60	S/H
4727.14578	0.60	0.25	0.87	A/U

of ∼0.1 Å. The H_β line from the UCLES spectrum is also shown in Fig. 3.

4 PHOTOMETRIC OBSERVATIONS

The photometric observations of ASAS-01 were carried out in the *V* and *I* bands with the 1.0-m Elizabeth telescope, located at the SAAO, and with the 0.41-m PROMPT-4 and PROMPT-5 robotic telescopes,[3] located at the Cerro Tololo Inter-American Observatory in Chile. A more detailed description of the observational settings, reduction procedure and calibration to a standard photometric system can be found in Hełminiak & Konacki (2011) and Hełminiak et al. (2011).

The majority of the SAAO observations were carried out in 2008 December. Most of the orbital phases were covered, but without the primary minimum in *V* and with only a few points in *I*. A clear out-of-eclipse modulation, probably originated by the presence of a cold spot, was noticed.

The PROMPT observations were carried out mostly in 2009 July, with two additional nights at the ends of August and September in the same year. This time, several primary minima were covered, but more points were collected around the secondary minimum. Again, we noticed an out-of-eclipse modulation, which was bascially the same as for the former SAAO data with regards to its shape.

The last small part of the data, mostly in *V*, comes from SAAO observations conducted in 2009 October. Again, a wide range of orbital phases was covered, including both minima, and an out-of-eclipse modulation was noticed to be of the same shape as for previous data sets. This led to the conclusion that if the modulation comes from the cold spots, the spot pattern did not change much between 2008 December and 2009 October.

In total, we gathered 598 brightness measurements in *V* and 586 in *I*, some under challenging conditions, which gave us a full phase coverage. Several primary and secondary minima, as well as an out-of-eclipse variation, were recorded, which allowed us to perform a detailed modelling of the system, starting from an update of the ephemeris and ending with spot and third-light properties. For the last purpose, we found the SAAO observations from 2008 December to be especially useful, where in good seeing conditions we were able to distinguish components A and B on the CCD images (Fig. 1). From a number of images where the components were well detached, we estimated their brightness ratio in both bands. In this way, we deduced that eclipses occur in the brighter component A, and we obtained reasonable starting values for the third-light contribution, which were later incorporated in the model.

5 PHYSICAL MODEL

The modelling procedure was, in many aspects, identical to the procedures described in the three previous papers of this series. We used the JKTEBOP code (Southworth, Maxted & Smalley 2004a; Southworth et al. 2004b), which is based on the Eclipsing Binaries Orbit Program (EBOP; Popper & Etzel 1981; Etzel 1981), and PHOEBE (Prša & Zwitter 2005) – an implementation of the WD code (Wilson & Devinney 1971). The JKTEBOP was used on the ASAS light curve and it served mainly to correct the ASAS ephemeris and to check for marks of a non-zero eccentricity. We did not use it extensively because it does not allow for spots or work on RV curves. We should also note that the PROMPT and SAAO light curves are almost indistinguishable and that the initial fits performed separately gave similar results. Thus, we decided to use all photometric data sets simultaneously in the whole fitting process. The photometric data points were weighted by their formal errors. The absolute values of several physical parameters, such as radii, bolometric magnitudes

[3] The Panchromatic Robotic Optical Monitoring and Polarimetry Telescopes (PROMPT) are operated by SKYNET – a distributed network of robotic telescopes located around the world, dedicated for continuous gamma-ray burst afterglow observations (http://skynet.unc.edu).

and distance, were obtained with the JKTABSDIM code, available with JKTEBOP, in the same way as described in previous papers.

We improved the ephemeris from JKTEBOP with PHOEBE using all available data, and we used them to create a final orbital fit (Section 3), and later the full solution. We set the third-light level in both bands to the values obtained from the CCD images and we allowed them to be fitted for in the later stages of the process. We have considered the uncertainty in the third-light level as the main source of errors of physical parameters, such as radii, temperatures and component magnitudes, in both bands (see also ASAS-08 in Hełminiak & Konacki 2011). The third-light uncertainty might possibly have its origin in the intrinsic photometric variability of component B, which is expected for such an active star.

The starting values of the effective temperatures were deduced from the empirical colour–temperature relations by Worthey & Lee (2011) on the basis of dereddened $V-I$ values for every component. For the dereddening, we used the $E(B-V) = 0.0145$ value from Schlegel, Finkbeiner & Davis (1998). In general, PHOEBE allows us to calculate fluxes in every passband separately for every star. If there are at least two light curves in various bands, the program also allows for fitting both effective temperatures simultaneously, using the concept of a binary effective temperature (Prša & Zwitter 2005). The treatment of limb darkening and reflection albedos is the same as in our previous papers, as well as the method of finding the parameters of cold spots. We have tested several different configurations, and we have found that the best solution is when a large cold spot is located on the secondary and is obscured during the secondary eclipse, and when there is a second small spot with maximum appearance around phase $\phi = 0.25$ on the primary. Because the light curves do not contain much information about the latitude of spots, we have decided to locate spots near the stars' equators and to keep these locations fixed. Moving towards other latitudes did not change the final model significantly – the difference in the inferred values of stellar parameters was smaller than the uncertainties coming from other sources. The final absolute values of the derived physical parameters of ASAS-01 A are given in Table 5. Fig. 4 presents the observational and modelled light curves in the V (left) and I (right) bands. We can see that the data taken with two different instruments and within almost a year overlap quite well, so we are justified in using these simultaneously. As mentioned before, the pattern of the spots did not change significantly during this time, and no short-scale evolution occurred, as has been found for two other low-mass systems, ASAS-09 and ASAS-21 (Hełminiak et al. 2011). The top and middle panels of Fig. 5 show a three-dimensional reconstruction of the eclipsing pair in three orbital phases: 0.04 (primary eclipse), 0.25 (quadrature) and 0.46 (secondary eclipse). Fig. 5 also shows the influence of spots on the light curve (bottom left) and RVs (bottom right). On the ΔRV plot, we also present RV residuals in the same form as in Fig. 2. We can see that the influence of spots on the RV curves is much smaller than the spread of measurements, which allows us to conclude that the uncertainty of the mass is not underestimated. We did not succeed in reaching a 3 per cent level of precision in mass and radius determination, but we were close (3.4–5.4 per cent).

Table 5. Absolute physical parameters of the ASAS-01 A eclipsing pair.

ASAS-01 A parameter	Primary Value	±	Secondary Value	±
i (°)	82 ± 2			
a ($R_\odot$)	2.502 ± 0.035			
M ($M_\odot$)	0.612	0.030	0.445	0.019
Ω	4.93	0.13	5.21	0.19
R ($R_\odot$)	0.596	0.020	0.445	0.024
$\log g$	4.68	0.31	4.79	0.45
$v_{\rm rot}$ (km s^{-1})[a]	67.3	2.5	50.5	2.8
$V-I$ (mag)[b]	1.84	0.14	2.17	0.14
$T_{\rm eff}$ (K)	3750	250	3085	300
$M_{\rm bol}$ (mag)	7.76	0.30	9.23	0.45
M_V (mag)	9.18	0.31	10.65	0.89
d (pc)	39 ± 6			
Parameters of spots				
Longitude (rad)[c]	0.20	0.05	4.71	0.07
Radius (rad)	0.7	0.1	0.3	0.08
Contrast	0.9	0.1	0.9	0.1

[a] In the case of synchronous rotation.
[b] Colour dereddened with $E(V-I) = 0.02$ mag.
[c] Counted counterclockwise, with 0 defined as the direction toward the companion star.

We can also see that our distance determination, 39(6) pc, is in very good agreement with the result obtained by Riaz et al. (2006). Assuming that the angular separation is 1.405(3) arcsec (Bergfors et al. 2010), the projected physical separation of components A and B is $\hat{a}_{\rm AB} = 55(8)$ au. This corresponds to an orbital period $P_{\rm AB} \simeq 333$ yr, assuming a circular orbit and the total mass of component B $M_{\rm B} \simeq 0.45$ $M_\odot$ (similar to $M_{\rm Ab}$ because it is almost exactly the same value of $V-I$), or 292 yr for $M_{\rm B} \simeq 0.9$ $M_\odot$ (see Section 6.2 for a discussion). The gravitational influence of component B on the pair A would not be detected with eclipse timing or precise RV measurements; however, the orbital motion of component B should be detectable with adaptive optics or various interferometric techniques.

6 DISCUSSION

6.1 Evolutionary status

We compare our results with three sets of theoretical isochrones: Yonsei–Yale (Y^2; Yi et al. 2001; Demarque et al. 2004), Dartmouth (Dotter et al. 2007) and Padova (Girardi et al. 2000; Marigo et al. 2008).

A comparison is shown in Fig. 6. We present the bolometric magnitude, radius, effective temperature, absolute V magnitude and the $V-I$ colour as a function of stellar mass. We compare our results with isochrones for an age of 1 Gyr and two cases of metallicities: (i) solar, $Z \simeq 0.02$ (red lines); (ii) above solar (green lines) – although different for every set, that is, $Z = 0.04$ for Y^2, 0.035 for Dartmouth and 0.03 for Padova. Because the accuracy of our measurements is worse than the canonical 3 per cent, the isochrones are shown only for comparison (i.e. we do not attempt to determine the age of the system). However, it is enough to conclude that ASAS-01 is probably a main-sequence object. The metallicity determination is even more insecure, but from Fig. 6 we can see that metallicities higher than solar are preferred. On the M versus $M_{\rm bol}$ and $\log T_{\rm eff}$ planes, the $Z > 0.02$ isochrones fit the data points significantly better.

The main-sequence evolutionary stage of ASAS-01 is confirmed by its galactic kinematics. We have used our determinations of the systemic velocity and distance together with the position and proper motion from the PPMXL catalogue: $\mu_\alpha = 120.4 \pm 4.0$ mas yr^{-1}, $\mu_\delta = -36.7 \pm 4.0$ mas yr^{-1} (Roeser, Demleitner & Schilbach 2010). The obtained values of $U = 3.3 \pm 2.3$ km s^{-1}, $V = -16.8 \pm 2.1$ km s^{-1} and $W = -7.8 \pm 2.3$ km s^{-1} put ASAS-01 in the

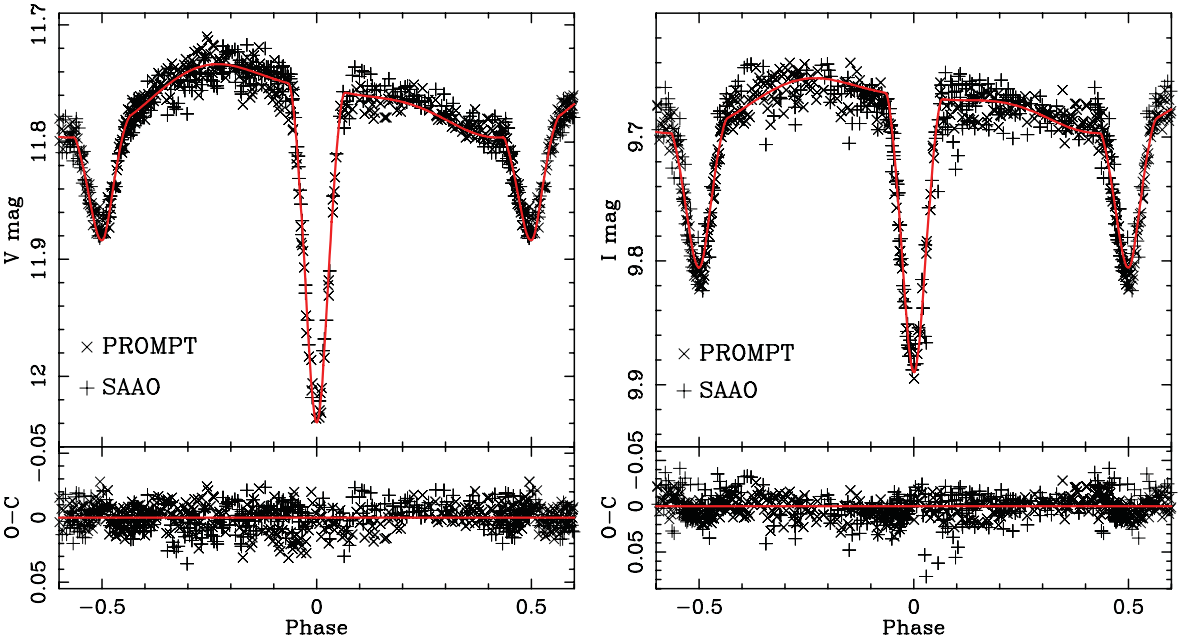

Figure 4. Observed *V*-band (left) and *I*-band (right) light curves of ASAS-01 obtained from our SAAO (+) and PROMPT (×) observations. An overplotted red line shows the best-fitting model. An out-of-eclipse light modulation, coming from the presence of two cold spots, is clearly visible. A significant change in the difference between the depths of the minima in the *V* and *I* bands indicates that the temperature ratio is substantially different from unity. Residua are plotted in the lower panels. A colour figure is available in the on-line version of the paper.

galactic thin disc, and only marginally in one of the young moving groups recently reported by Zhao, Zhao & Chen (2009, ID = 15 therein).

It is worth noticing that, on the *M*/*R* plane, the measurements agree within errors with the Y^2 and Dartmouth models. The second set of models, especially, seems to reproduce the physical properties of components A of ASAS-01. This is in contrast to many recent results found in studies of LMDEBs (see Kraus et al. 2011). The usually, but not always, observed characteristic of low-mass stars in close binaries is that theoretically predicted radii are smaller and temperatures are larger with respect to what is observed (Ribas et al. 2008); this situation is seen for the Padova models. The Dartmouth models also seem to follow this trend, but only by a few per cent. Within our uncertainties, they correctly predict the observed radii and, in the case of $Z = 0.035$, also temperatures. The deviation is smaller for the larger component, which presumably rotates faster. Thus, it does not support the possible radius–rotation relation for $M < 0.7\ \mathrm{M}_\odot$ stars (Kraus et al. 2011). At the same time, the properties of the secondary are very well reproduced by the Y^2 models (except for the colour), but for the primary we see a typical underestimation of the radius and an overestimation of the temperature. From this short discussion, we can only conclude that the Dartmouth models might be the best models to reproduce the properties of low-mass stars (see also Thompson et al. 2010), although discrepancies at the level of ∼3 per cent are present. However, this is significantly smaller than for the majority of previous studies where differences in the radii of 5–15 per cent were claimed.

6.2 Component B

Because we have the two components separated on the *V*- and *I*-band images (Fig. 1), and because the physical model is created with PHOEBE with the third light included, we have been able to estimate the photometric properties of component B. Table 6 presents the fractional fluxes in both bands, the dereddened $V - I$ colour and the absolute *V* magnitude.

Fig. 7 presents our measurements on the V–I/M_V plane. We use the data from Tables 5 and 6, and the same isochrones as in Fig. 6. We see that the Dartmouth set for $Z = 0.02$ again gives the best match for the eclipsing pair A. Component B is about 0.7 mag brighter but it has almost the same colour as Ab ($V - I = 2.14$ mag). Because of the relatively large errorbars (magnified mainly by the uncertainty in the third-light parameter in our model), we can formally find that the *V* magnitudes of B and Ab are almost equal and that they are still consistent with the considered Dartmouth and both Y^2 isochrones. However, if we assume that component B is composed of two, nearly twin stars with masses ∼0.45–0.5 $\mathrm{M}_\odot$, which would thus have $V - I$ colour around 2.15 mag (i.e. almost the same as the value observed for B), in Fig. 7 these putative Ba and Bb components would be located at the position marked by the empty square (lowering the flux by a factor of 2 increases the magnitude by ∼0.7). In such a situation, the Dartmouth $Z = 0.02$ and Y^2 isochrones would reproduce the observed properties of the system much better. We consider that this fact supports the hypothesis of the binarity of ASAS-01 B.

The binarity of component B, with a mass ratio close to 1 and with component colours close to the value observed, is consistent with the fact that no marks of additional eclipses are found in our *V*- and *I*-band light curves. From the orbital fit for the RVs of component B, presented in Table 3, we can estimate the orbital inclination i_B for various values of the mass ratio q_B and the desired mass of the more massive component M_Ba. We present these calculations in Table 7.

For a number of different values of q_B, we present values of $M \sin^3 i_\mathrm{B}$ for Ba and Bb, and values of inclination angles, for which $M_\mathrm{Ba} = 0.45$ or $0.5\ \mathrm{M}_\odot$. From Table 7, we can see that if ASAS-01 B is a binary, in order to explain all the observed properties we need the inclination angle i_B to be between 50° and 70°, which corresponds to $q \geq 0.8$. For these mass values of Ba and Bb, we can expect the observed colour to be around the value given in Table 6.

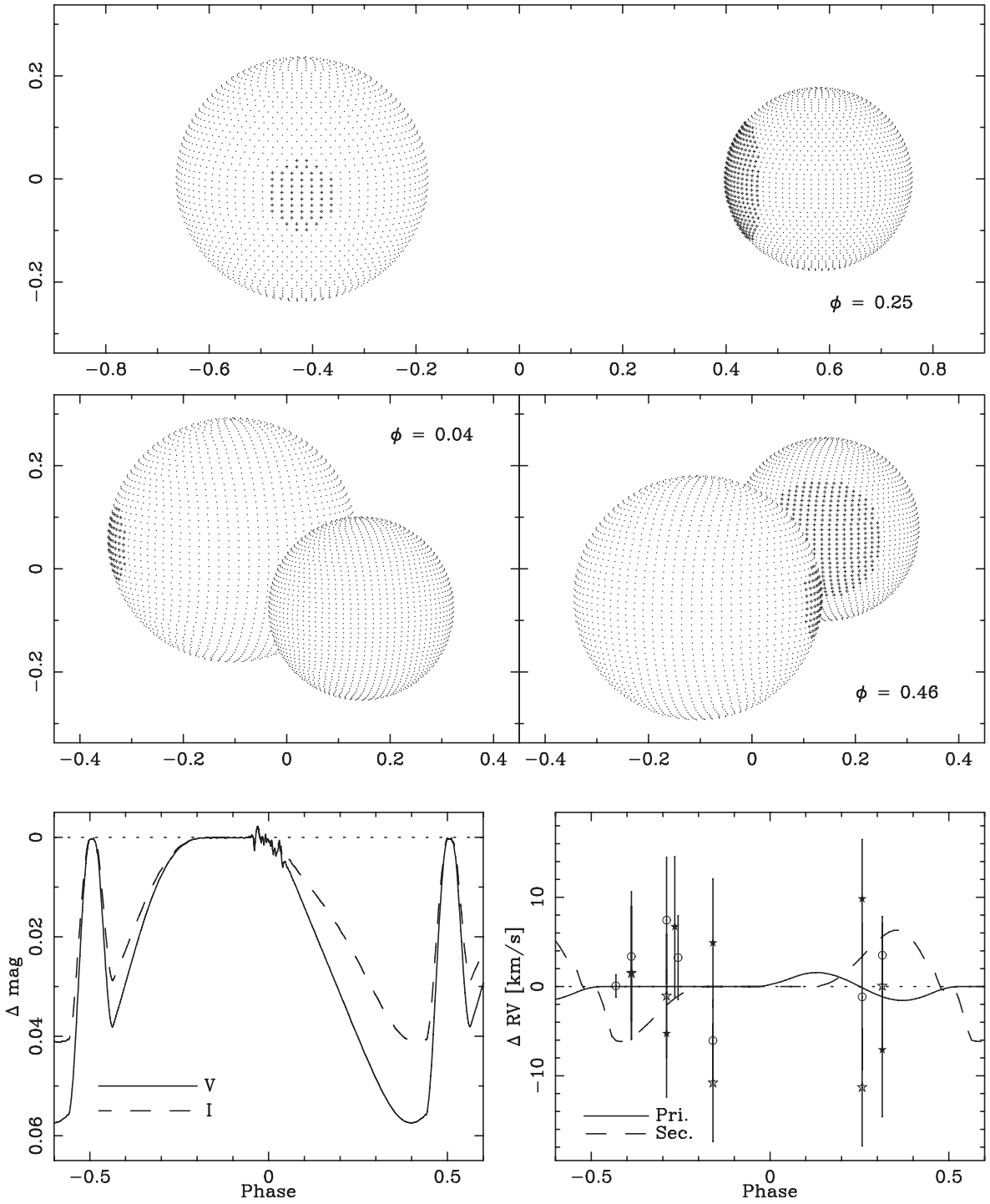

Figure 5. Top and middle: three-dimensional reconstruction of the ASAS-01 A eclipsing binary, based on our best-fitting model in quadrature (top) and during eclipses (middle). Dimensions are scaled so that $a = 1$. Bottom: influence of spots on the light curves (left) in the V (solid line) and I (dashed line) bands, and on the RV curves of the primary (solid) and secondary (dashed) components. In the RV panel, we also plot the residua of the model, in the same way as in Fig. 2. In the LC panel, the large scatter on the V curve around $\phi \sim 0$ comes from the sampling of the stellar surface used in the PHOEBE code.

Assuming lower values of q_B, we would end up in a situation where additional eclipses occur and the Bb component is significantly fainter. In such a case, the total brightness of ASAS-01 B would be lower than observed, but still within relatively large error bars.

If ASAS-01 is a double–double system, it would join a small group of interesting objects of this type. To date, only two other LMDEBs are known to be in a similar configuration: BD -22 5866, which is a system with a K7+K7 eclipsing pair and an M1+M2 non-eclipsing binary (Shkolnik et al. 2008), and YY Gem, which is the faintest member of a sextuple system, composed of three spectroscopic binaries, Castor A, B and C (α Gem ABC; Vinter Hansen, Neubauer & Roosen-Raad 1940; Kron 1952; Bopp 1974). There are also a few examples of LMDEBs known to have a single additional companion, such as LP 133-373 (Vaccaro et al. 2007),

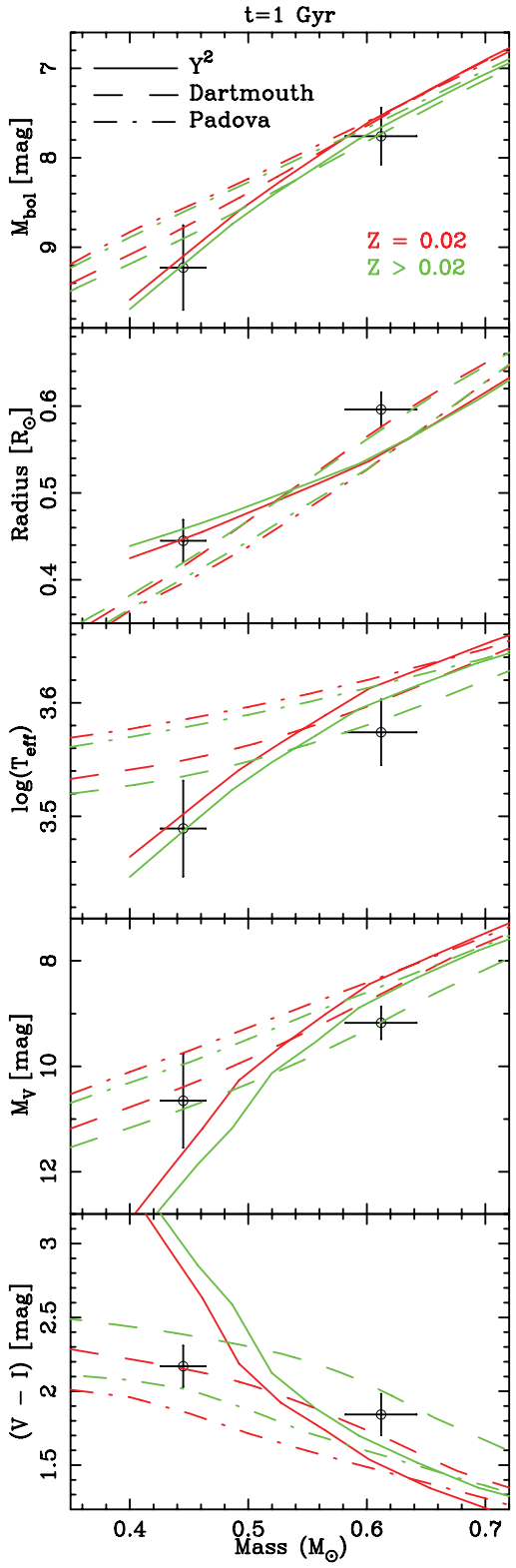

Figure 6. Comparison of our results for the ASAS-01 A eclipsing pair with theoretical 1-Gyr isochrones on mass M versus (from top to bottom) bolometric magnitude, radius, effective temperature, absolute V magnitude and $V - I$ colour. The Y^2, Dartmouth and Padova isochrones are depicted by solid, dashed and dot-dashed lines, respectively. Isochrones for solar metallicity ($Z \simeq 0.02$) are shown in red and those for higher Z are shown in green. A colour version of the figure is available in the on-line version of the paper.

Table 6. Photometric properties of component B from the PHOEBE model.

Parameter	Value	±
$F_{V,3}$ (per cent)[a]	34.8	1.5
$F_{I,3}$ (per cent)[a]	42.9	3.2
$(V-I)_3$ (mag)[b]	2.15	0.13
$M_{V,3}$ (mag)	10.82	0.70

[a] Fractional fluxes defined as a percentage of the flux of component A.
[b] Colour dereddened with $E(V - I) = 0.02$ mag.

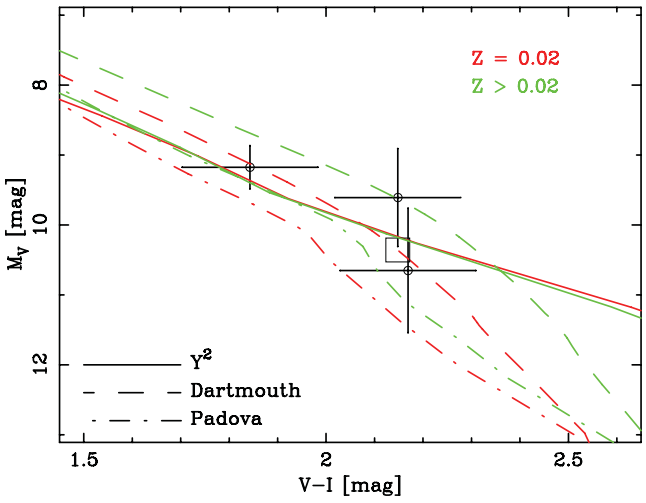

Figure 7. Colour–brightness diagram with our measurements for the Aa, Ab and B components of ASAS-01, together with theoretical 1-Gyr isochrones. The line and colour coding is the same as in Fig. 6. The square shows the approximate position of the components of ASAS-01 B if it were composed of two identical stars showing the same $V - I$ value as observed. A colour version of the figure is available in the on-line version of the paper.

Table 7. Values of the inclination of the putative orbit of component B for various values of q_B and the masses of the more massive component of 0.45 $M_\odot$ ($i_{B,0.45}$) and 0.5 $M_\odot$ ($i_{B,0.5}$). The mass function is taken from Table 3. Note that $f(M_{Ba}) = 0.0565(92)\ M_\odot$.

q_B	$M_{Ba} \sin^3 i_B$ ($M_\odot$)	$M_{Bb} \sin^3 i_B$ ($M_\odot$)	$i_{B,0.45}$ (°)	$i_{B,0.5}$ (°)
1.00	0.226	0.226	53	50
0.95	0.251	0.238	55	53
0.90	0.280	0.252	59	56
0.85	0.315	0.268	63	59
0.80	0.358	0.286	68	63
...				
0.718	0.45	0.323	90	75
0.684	0.5	0.342	––	90

HIP 96515[4] (Huélamo et al. 2009), MR Del (Pribulla et al. 2009; Djurašević et al. 2011), NLTT 41135 (Irwin et al. 2010), ASAS-08 (Montes et al. 2007; Hełminiak & Konacki 2011) or the triply eclipsing KOI-126 (Carter et al. 2011). Such systems not only allow more rigid constraints on the evolutionary models than in the cases

[4] No RV curve is published for this system.

of 'lonely' eclipsing binaries, but they also play an important role in testing star-formation theories, stellar population codes and dynamical interactions in multiple stellar systems. The relative brightness and small distance to ASAS-01 make it a valuable object for further studies.

7 SUMMARY

As a result of our analysis of the components of ASAS-01, an M-type multiple system, we have obtained a complete set of orbital and physical parameters of the detached eclipsing pair A, and the photometric and spectroscopic properties of component B. Because of a number of difficulties, our results have an accuracy of 3–6 per cent, which is not enough for performing a reliable estimation of the evolutionary status of the system. Within the error bars, however, we might be able to reproduce our results with main-sequence theoretical models. The observed spectroscopic and photometric properties of component B of the system suggest that this is a binary composed of nearly identical stars. However, the eventual orbital solution is uncertain, and the M_V and $V - I$ errors are quite large. Thus, we cannot make any final conclusions on this topic. As a member of a rare class of late-type multiples with eclipsing detached components, ASAS-01 should be considered as a potential test bed for stellar formation and evolution theories. It definitely deserves more attention and investigation, especially considering the system's spectroscopy and the photometric properties of component B.

ACKNOWLEDGMENTS

We would like to thank David Laney, John Menzies and Hannah Worters from the SAAO for their support during our observations there. We also thank Stephen Marsden and the Anglo-Australian Observatory astronomers for their help during our observing runs on the AAT. We are grateful to Samba Fall and Chelsea Harrison for careful proofreading and corrections of this manuscript.

This research was co-financed by the European Social Fund and the national budget of the Republic of Poland within the framework of the Integrated Regional Operational Programme, Measure 2.6, Regional innovation strategies and transfer of knowledge, which is an individual project of the Kuyavian–Pomeranian Voivodship 'Scholarships for PhD students 2008/2009 – IROP'. This work is supported by the Polish National Science Center grant 5813/B/H03/2011/40, by the Foundation for Polish Science through a FOCUS grant and fellowship and by the Polish Ministry of Science and Higher Education through grants N203 005 32/0449, N203 3020 35 and N203 379936. KGH acknowledges support provided by the Proyecto FONDECYT Postdoctoral No. 3120153, the Centro de Astrofísica FONDAP Proyecto 15010003, Comité Mixto ESO-Chile and by the Ministry for the Economy, Development, and Tourism's Programa Iniciativa Científica Milenio through grant P07-021-F, awarded to The Milky Way Millennium Nucleus. MWM acknowledges support from the Townes Fellowship Program, an internal UC Berkeley SSL grant, and the State of Tennessee Centers of Excellence programme. This research was supported in part by the National Science Foundation under Grant No PHY05-51164 and through Grants 0959447, 0836187, 0707634 and 0449001. The observations on the AAT/UCLES have been funded by the Optical Infrared Coordination Network (OPTICON), a major international collaboration supported by the Research Infrastructures Programme of the European Commission's Sixth Framework Programme.

This research has made use of the Simbad data base, operated at CDS, Strasbourg, France.

REFERENCES

Beers T. C., Rossi S., Ulrich D., Wilelm R., 1996, AJ, 112, 1188
Bergfors C. et al., 2010, A&A, 520, A54
Blake C. H., Torres G., Bloom J. S., Gaudi B. S., 2008, ApJ, 684, 635
Bopp B. W., 1974, ApJ, 193, 389
Carter J. A. et al., 2011, Sci, 331, 562
Chabrier G., Gallardo J., Baraffe I., 2007, A&A, L17
Clausen J. V., Torres G., Bruntt H., Andersen J., Nordström B., Stefanik R. P., Latham D. W., Southworth J., 2008, A&A, 487, 1095
Demarque P., Woo J-H., Kim Y-C., Yi S. K., 2004, ApJS, 155, 667
Djurašević G., Yilmaz M., Baştürk Ö., Kiliçoğlu T., Latković O., Çalişkan Ş., 2011, A&A, 525, A66
Dotter A., Chaboyer B., Jevremović D., Baron E., Ferguson J. W., Sarajedini A., Anderson J., 2007, AJ, 134, 376
Etzel P. B., 1981, in Carling E. B., Kopal Z., eds, Photometric and Spectroscopic Binary Systems. Reidel, Dordrecht, p. 111
Gioia I. M., Maccacaro T., Schild R. E., Wolter A., Stocke J. T., Morris S. L., Henry J. P., 1990, ApJS, 72, 567
Girardi L., Bressan A., Bertelli G., Chiosi C., 2000, A&AS, 141, 371
Halbwachs J. L., Mayor M., Udry S., Arenou F., 2003, A&A, 397, 159
Hełminiak K. G., Konacki M., 2011, A&A, 526, A29
Hełminiak K. G., Konacki M., Muterspaugh M. W., Ratajczak M., 2009, MNRAS, 400, 969
Hełminiak K. G. et al., 2011, A&A, 527, A14
Huélamo N. et al., 2009, A&A, 503, 873
Irwin J. et al., 2010, ApJ, 718, 1353
Irwin J. et al., 2011, ApJ, 742, 123
Kraus A. L., Tucker R. A., Thompson M. I., Craine E. R., Hillenbrand L. A., 2011, ApJ, 728, 48
Kron G. E., 1952, ApJ, 115, 301
Lacy C., 1977, ApJ, 218, 444
Lucy L. B., 2006, A&A, 457, 629
Marigo P., Girardi L., Bressan A., Grönewegen M. A. T., Silva L., Granato G. L., 2008, A&A, 482, 883
Montes D., Crespo-Chacón I., Gálvez M. C., Fernández-Figueroa M. J., 2007, in Hartkopf W. I., Guinan E. F., Harmanec P., eds, Proc. IAU Symp. 240, Binary Stars as Critical Tools & Tests in Contemporary Astrophysics. Cambridge University Press, Camridge, p. 690
Parihar P., Messina S., Bama P., Medhi B. J., Muneer S., Velu C., Ahmad A., 2009, MNRAS, 395, 593
Pojmański G., 2002, Acta Astron., 52, 397
Popper D. M., Etzel P. B., 1981, AJ, 86, 102
Pribulla T. et al., 2009, AJ, 137, 3655
Prša A., Zwitter T., 2005, ApJ, 628, 426
Riaz B., Gizis J. E., Harvin J., 2006, AJ, 132, 866
Ribas I., Morales J. C., Jordi C., Baraffe I., Chabrier G., Gallardo J., 2008, MmSAI, 79, 562
Roeser S., Demleitner M., Schilbach E., 2010, AJ, 139, 2440
Schlegel D., Finkbeiner D., Davis M., 1998, ApJ, 500, 525
Shkolnik E., Liu M. C., Reid I. N., Hebb L., Cameron A. C., Torres C. A., Wilson D. M., 2008, ApJ, 682, 1248
Southworth J., Maxted P. F. L., Smalley B., 2004a, MNRAS, 351, 1277
Southworth J., Zucker S., Maxted P. F. L., Smalley B., 2004b, MNRAS, 355, 986
Stocke J. T., Morris S. L., Gioia I. M., Maccacaro T., Schild R., Wolter A., Fleming T. A., Henry J. P. J., 1991, ApJS, 76, 813
Szczygieł D., Socrates A., Paczyński B., Pojmański G., Pilecki B., 2008, Acta Astron., 58, 405
Thompson I. B., Kałużny J., Ruciński S. M., Krzemiński W., Pych W., Dotter A., Burley G. S., 2010, AJ, 139, 329
Torres G., Ribas I., 2002, ApJ, 567, 1140

Vaccaro T. R., Rudkin M., Kawka A., Vennes S., Oswalt T. D., Silver I., Wood M., Allyn Smith J., 2007, ApJ, 661, 1112
Vinter Hansen J. M., Neubauer F. J., Roosen-Raad D., 1940, Lick Obs. Bull., 19, 89
Voges W. et al., 1999, A&A, 349, 389
Wilson R. E., Devinney E. J., 1971, ApJ, 166, 605
Worthey G., Lee H-c., 2011, ApJS, 193, 1
Yi S. K., Demarque P., Kim Y-C., Lee Y-W., Ree C. H., Lejeune T., Barnes S., 2001, ApJS, 136, 417
Zhao J., Zhao G., Chen Y., 2009, ApJ, 692, L113
Zucker S., Mazeh T., 1994, ApJ, 420, 806

This paper has been typeset from a TEX/LATEX file prepared by the author.